analyzed using a VG PlasmaQuad LA-ICP-MS, with a 213-nm laser, and using a Cameca ims 6f ion probe. For details, see C. M. O'D. Alexander [*Geochim. Cosmochim. Acta* **58**, 3451 (1994)].
20. M. K. Weisberg *et al.*, *Meteorit. Planet. Sci.* **33**, A166 (1998).
21. M. K. Weisberg *et al.*, *Meteorit. Planet. Sci.*, in press.
22. A. N. Krot *et al.*, *Lunar Planet. Sci.* **31**, #1499 (2000) [CD-ROM].
23. A. N. Krot *et al.*, *Lunar Planet. Sci.* **31**, #1448 (2000) [CD-ROM].
24. A. J. Greshake, A. N. Krot, A. Meibom, K. Keil, *Meteorit. Planet. Sci.* **35**, A65 (2000).
25. A. Meibom *et al.*, *Science* **288**, 839 (2000).
26. J. T. Wasson (personal communication) questioned the classification of metal-rich CH and Bencubbin-like (HH 237 and QUE) meteorites as primitive carbonaceous chondrites and suggested that their unusual mineralogical and chemical characteristics could have resulted from melting, vaporization, outgassing, condensation, and size-sorting in a cloud of impact ejecta on the CR parent asteroid. According to this hypothesis, Ca- and Al-rich inclusions (CAIs) in CH and Bencubbin-like chondrites either survived this impact event or were added later during regolith gardening together with "normal" chondrules of porphyritic textures. The latter scenario can be excluded, because such "normal" chondrules are absent in HH 237 and QUE. Furthermore, the observed differences in mineralogy and chemistry of CAIs in CR, CH, and Bencubbin-like meteorites exclude a common source from the CR parent asteroid (*27*).
27. A. N. Krot *et al.*, in preparation.
28. M. I. Petaev, A. Meibom, A. N. Krot, J. A. Wood, K. Keil, *Meteorit. Planet. Sci.* **36**, 93 (2001).
29. A. J. Campbell, M. Humayun, A. Meibom, A. N. Krot, K. Keil, *Geochim. Cosmochim. Acta* **65**, 163 (2001).
30. The term "dust" is defined as a solid phase containing all elements but H and noble gases in cosmic proportions, and the dust/gas ratio as the atomic Si/H ratio normalized to the solar Si/H ratio of 3.58×10^{-5}. Note that astrophysicists conventionally define the dust/gas ratio as the mass of the dust component divided by the mass of gas component. According to this definition, the solar dust/gas ratio is ~0.005. See also (*35*).
31. The zoned FeNi metal grains in HH 237 and QUE contain three to four times less Cr than does metal condensed from a gas of solar composition, suggesting condensation under relatively oxidizing conditions, which could have resulted from complete evaporation of a solar nebula region with enhanced dust/gas ratios of ~10 to 50× solar (*28, 30*).
32. A. Meibom *et al.*, *Meteorit. Planet. Sci.* **35**, A107 (2000).
33. A. J. Campbell, M. Hymayun, M. K. Weisberg, *Meteorit. Planet. Sci.* **35**, A38 (2000).
34. G. F. Herzog *et al.*, *Meteorit. Planet. Sci.* **35**, A71 (2000).
35. E. Anders, N. Grevesse, *Geochim. Cosmochim. Acta* **53**, 197 (1989).
36. J. Zipfel, F. Wlotzka, B. Spettel, *Lunar Planet. Sci.* **29**, #1417 (1998) [CD-ROM].
37. R. H. Hewins, *Geochim. Cosmochim. Acta* **55**, 935 (1991).
38. Silicate inclusions inside chemically zoned FeNi metal grains are texturally and compositionally similar to the CC chondrules, but tend to have higher Cr_2O_3 (1.1 ± 0.5 wt %) as a result of mild redistribution of Cr between metal and enclosed silicates by solid-state diffusion at high temperatures during FeNi metal condensation.
39. A. N. Krot, B. Fegley Jr., H. Palme, K. Lodders, in (*2*), pp. 1019–1055.
40. H. C. Connolly Jr., R. H. Hewins, *Geochim. Cosmochim. Acta* **59**, 3231 (1995).
41. D. Ebel, L. Grossman, *Geochim. Cosmochim. Acta* **64**, 339 (2000).
42. S. S. Russell, A. N. Krot, A. Meibom, C. M. O'D. Alexander, T. E. Jeffries, *Meteorit. Planet. Sci.* **35**, A139 (2000).
43. F. H. Shu, H. Shang, T. Lee, *Science* **271**, 1545 (1997).
44. F. H. Shu, H. Shang, M. Gounelle, A. E. Glassgold, T. Lee, *Astrophys. J.*, in press.
45. D. S. Woolum, P. Cassen, *Meteorit. Planet. Sci.* **34**, 897 (1999).
46. Supported in part by NASA grants NAG 5-412 (K. Keil, principal investigator), NAG 5-4225 (C. M. O'D. Alexander, principal investigator), and OSS (A. N. Krot, principal investigator). We thank the Meteorite Working Group, the Smithsonian Institution, M. Weisberg, and J. Zipfel for supplying samples. F. Shu and an anonymous reviewer are thanked for constructive reviews that helped improve the manuscript. A.M. is grateful for support from the Danish Natural Science Research Council. This is HIGP publication 1134 and SOEST publication 5335.

8 December 2000; accepted 22 January 2001

High Geomagnetic Intensity During the Mid-Cretaceous from Thellier Analyses of Single Plagioclase Crystals

John A. Tarduno,* Rory D. Cottrell, Alexei V. Smirnov

Recent numerical simulations have yielded the most efficient geodynamo, having the largest dipole intensity when reversal frequency is low. Reliable paleointensity data are limited but heretofore have suggested that reversal frequency and paleointensity are decoupled. We report data from 56 Thellier-Thellier experiments on plagioclase crystals separated from basalts of the Rajmahal Traps (113 to 116 million years old) of India that formed during the Cretaceous Normal Polarity Superchron. These data suggest a time-averaged paleomagnetic dipole moment of $12.5 \pm 1.4 \times 10^{22}$ amperes per square meter, three times greater than mean Cenozoic and Early Cretaceous–Late Jurassic dipole moments when geomagnetic reversals were frequent. This result supports a correlation between intervals of low reversal frequency and high geomagnetic field strength.

If there is an inverse relationship between reversal rate and paleointensity (*1*, *2*), it should be most obvious during geomagnetic superchrons, times during which the field apparently remains in one polarity for tens of millions of years. In particular, intensities during the 37-million-year long Cretaceous Normal Polarity Superchron should be higher than those of the Cenozoic or pre–mid-Cretaceous. However, there are few paleointensity results for the mid-Cretaceous (*3–5*). Thellier-Thellier (*6*) experiments often fail on whole rock basalt samples because of alteration during the successive heating steps required by the method. Results from mid-Cretaceous rocks that pass reliability checks are often not sufficiently numerous to average secular variation at the collection site.

Recently we have developed an approach to measure paleointensity using single plagioclase crystals separated from basalts (*7*, *8*). These crystals are affected less by experimental alteration (*7*, *8*). Analyses of magnetic separates by transmission electron microscopy reveal that these crystals contain single to pseudo–single-domain inclusions (50 to 250 nm) (*7*). In a test of the method, Thellier-Thellier analyses of plagioclase crystals from a 1955 flow from Kilauea volcano, Hawaii, yielded paleointensity estimates that agreed within error with those derived from the relatively fresh whole rocks (*9*) and magnetic observatory data (*7*).

The potential of measuring plagioclase for paleointensity analysis is best seen in older rocks where clays are ubiquitous. In a study of a single lava flow from the mid-Cretaceous [113 to 116 million years ago (Ma)] Rajmahal Traps of eastern India (*10*), Cottrell and Tarduno (*8*) show that directional data from oriented plagioclase crystals match those from the whole rock. Thermal demagnetization and magnetic hysteresis properties suggest that the plagioclase crystals and whole rocks have a similar, titanomagnetite mineralogy. Magnetic inclusions in the crystals are equant to rectangular, 100 to 350 nm in length, and not strongly aligned within the crystals (as indicated by hysteresis properties measured at different crystal orientations).

Magnetic hysteresis data (*8*) also indicate that a fine-grained magnetic phase forms in the whole rocks as a result of Thellier-Thellier heatings. The source of this fine-grained material is thought to be the alteration of clay in the whole rock ground mass. This behavior is not seen in the plagioclase crystals. This difference is reflected in the quality of the paleointensity results and their absolute value. Data from whole rocks often fail to meet reliability criteria. They generally

Department of Earth and Environmental Sciences, University of Rochester, Rochester, NY, 14627, USA.

*To whom correspondence should be addressed. E-mail: john@earth.rochester.edu

yield lower paleofield values, which can be attributed to the growth of new magnetic minerals (*8*).

These results indicate that in the Rajmahal basalts, paleointensity data derived from plagioclase crystals yield more reliable paleofield estimates than those from whole rocks (*11*). But results from a single lava flow represent only an instantaneous field record. To draw conclusions relevant to the geodynamo, records that average secular variation are required. We report here results of a comprehensive paleointensity study of plagioclase crystals from the Rajmahal Traps that yield such a record.

The Rajmahal Trap lavas, exposed in the Rajmahal Hills of West Bengal and Bihar, are mainly quartz tholeiites. Most of the thicker exposed sections are in the range of 100 to 250 m, sometimes containing one or more interbeds of lacustrine sediments. These rocks represent erosional remnants of what was probably once a much more extensive large igneous province.

Our samples come from sites in the southern and northern Rajmahal Hills (near Rampur Hat and Sahibganj, respectively). Samples were collected as field drilled cores and were oriented with a Sun compass. Site locations were recorded by hand-held global positioning system (GPS) units (Web table 1) (*12*). Exposures in the south were limited to isolated large quarries and river cuts. Here lava flows >10 m thick are common, with well-developed columnar jointing. One of our sites (RS7/8) is diabase, likely a sill, emplaced near the base of the Rajmahal lavas, close to their contact with Gondwana group sediments. Site RS10 also occurs in the lower part of the trap succession. Our northern samples are from a small quarry near the town of Lilitari and were collected in a stratigraphic section. Lavas in this area are not as uniformly thick as in the south. We observed thin, 1-m flows interbedded with thicker 5- to 10-m flows. An ~8-m sedimentary interbed occurs midway in the section, separating sites RM2 and RM6 from RM14, 15, and 16. Each site was collected in a separate lava flow.

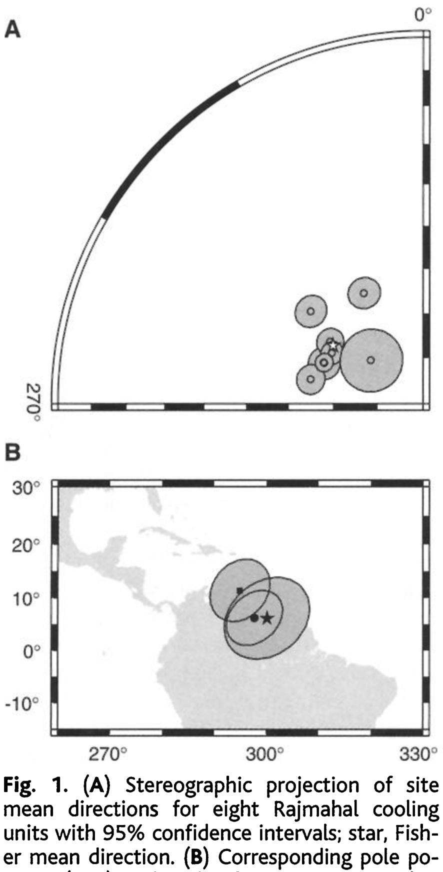

Fig. 1. **(A)** Stereographic projection of site mean directions for eight Rajmahal cooling units with 95% confidence intervals; star, Fisher mean direction. **(B)** Corresponding pole position (star) with poles from previous studies with 95% confidence intervals. Solid circle, Klootwijk (*15*); square, Sherwood and Mallik (*13*).

All paleomagnetic direction and paleointensity measurements were done at the University of Rochester with a direct current superconducting quantum interference device magnetometer with a 4-cm access and a high-resolution sensing coil configuration. Standard thermal demagnetization of whole rocks (25°C increments) shows similar behavior to that described in previous studies (*8*, *13*), consistent with a titanomagnetite carrier. We have found, however, that secondary components are not removed until treatments slightly higher (*8*) (250° to 300°C for thermal demagnetization; 20 to 25 mT for alternating field demagnetization) than those recognized in earlier works.

Results from the nine sites reported here are of normal polarity and are based solely on the thermal demagnetization data. Directions from sites RM14 and RM15 (adjacent lava flows) were indistinguishable and were therefore combined in further analyses. The site declinations and inclinations from the eight time-independent units are Fisherian distributed at the 90% (M_u = 1.193) and 95% (M_e = 0.759) confidence level (*14*). These results indicate a mean pole position similar to that of previous studies (*13*, *15*) (Fig. 1).

We calculated the angular dispersion of the data, S

$$S^2 = \frac{1}{N-1}\sum_{i=1}^{N}\Delta_i^2 \qquad (1)$$

where N is the number of virtual geomagnetic poles (VPGs) and Δ_i is the angle between the i VGP and the mean VGP. The angular dispersion (S = 11.7 $^{+6.7°}_{-3.2°}$; 95% confidence interval) indicated is less than would be expected from VGP data of the past 5 million years. Because paleosecular variation has changed with time (*1*), however, we must compare our estimate with data of similar age. We compare our results with the global summary of McFadden *et al.* (*16*), who report VGP angular dispersion values for the Cretaceous Normal Polarity Superchron between 80 and 110 Ma. Although this interval may include some reversed polarity Late Cretaceous data, it nevertheless provides the best available gauge of the mean angular dispersion during the mid-Cretaceous. Our value from the Rajmahal Traps is within error of that predicted (*16*). This suggests that at least several millennia are recorded by our data. The available age data (*10*), together with our geological sampling, suggest that an interval 100,000 to 1 million years long has been sampled.

The experimental methods used for paleointensity determinations follow those described by Cottrell and Tarduno (*7*, *8*). Plagioclase crystals were picked from basalt samples crushed with a ceramic mortar and pestle and then washed and sonicated with distilled water. Crystals used in subsequent experiments ranged in size from 0.5 to 2.0 mm in their longest dimension and are free of groundmass and clear when viewed optically (Fig. 2). Cleaned crystals with natural remanent magnetization (NRM) intensities $>\sim 5 \times 10^{-11}$ A/m² were chosen for paleointensity measurements. These crystals were set inside pressed salt pellets (0.5-inch diameter).

Applied fields of 40 and 60 μT were used in a thermal demagnetization oven for the Thellier-Thellier experiment. No significant differences were seen in data obtained with these two applied field values (*8*). We use the version of this experiment discussed by Coe (*17*). The plagioclase crystals were heated for 25 to 30 min and cooled for an equivalent interval. Temperature steps of 50°C were used for the first 250°C (the unblocking temperature range of the viscous overprint magnetization seen in our samples), followed by demagnetization and partial thermoremanent magnetization (pTRM) acquisition at 25°C increments until >90% of the NRM was lost or the magnetizations were no longer stable. Examples of data derived from single crystals are shown in Fig. 2.

Several criteria were used to judge the quality of the paleointensity data. Successful trials must show a linear relationship between NRM-lost and TRM-gained, where the slope of the line is the ratio of the ancient field to the applied field. Least squares analysis was used to fit the data. Four or more points must define the best fit line with $R^2 > 0.90$. A large percentage of the primary component remanence (typically >50%) must be lost within the temperature range defined by the best fit line. Several pTRM checks were performed to test for alteration. To be judged successful, a pTRM check must fall within 5% of the original TRM value. Least squares fit to the directional data of the field-off steps of the modified Thellier-Thellier technique must also have a mean angular dispersion of less than 15° and tend toward the origin in orthogonal vector plots. In addition, the inclination direction of the field-off steps should not tend toward the applied field direction.

Changes in NRM and TRM intensities during the Thellier-Thellier experiments are generally very small (sometimes $<5 \times 10^{-12}$ A/m^2). Background measurements on the superconducting rock magnetometer range from 4 to 8×10^{-13} A/m^2. Typical sample holders have a slightly higher range (1 to 5×10^{-12} A/m^2). A blank salt pellet can have intensities ranging from 0.5 to 1.5×10^{-11} A/m^2. To reduce the influence of measurement noise, particularly for steps at higher temperatures where intensities are extremely low, we used a three-point sliding average of NRM and TRM intensities over the optimal temperature range identified in the orthogonal vector plots. These averaged data were used in assessing the quality of the data through reliability checks and in the calculation of final paleointensities. The NRM-TRM unaveraged data sometimes have gaps that are not present in the averaged data. However, these gaps correspond to the range of Curie temperatures measured on the Rajmahal basalts (*7*) and therefore simply record intervals of rapid NRM loss with heating. A statistic commonly used to measure such data gaps (*18*, *19*) is similar between the unaveraged ($g = 0.68 \pm 0.12$) and averaged data ($g = 0.78 \pm 0.06$). Moreover, using t tests (*20*), we cannot reject the null hypothesis that the paleointensity means of the averaged and unaveraged site data are the same at the 95% confidence level (*8*).

Fifty-six of the 149 crystals measured met the selection criteria. The NRMs of 30% of the crystals after heating to relatively low temperatures (~150°C) dropped rapidly, and further analyses of paleointensity were impractical. These crystals probably acquired a relatively strong isothermal remanent magnetization (IRM) during sample preparation. Twenty-seven of the crystals behaved erratically throughout the experiment and were rejected. Viscous magnetizations (VRMs), especially those acquired when moving samples in the presence of the Earth's field between the oven and magnetometer, are probably the dominant source of noise for this erratic behavior. Thirteen crystals did not have field-off steps that tended toward the origin of orthogonal vector plots, and the field-off inclinations from eight crystals tended toward the direction of the applied field at relatively low unblocking temperatures.

Averaged data meeting reliability criteria described above are available from multiple samples of the eight time-independent units (Fig. 3; Web tables 1 to 3) (*12*). Together these data yield a mean intensity of 77.6 ± 9.4 μT (1σ error). This value corresponds to a virtual dipole moment (VDM) of 12.5×10^{22} Am^2 $\pm$ 1.4×10^{22} Am^2 (1σ). These values are not significantly different from those obtained fitting the unaveraged data, which are 74.5 ± 9.6 μT and $12.2 \pm 1.6 \times 10^{22}$ Am^2 (1σ) for field and VDM values, respectively.

Because the directions from the cooling units indicate that secular variation has been averaged, the mean paleointensity can be considered a paleomagnetic dipole moment, rather than a virtual dipole moment. Thellier-Thellier results from basalts (*21–26*) with coincident directional data demonstrating that a paleomagnetic dipole moment has been recorded are rare for rocks older than 1 million years (Fig. 4). Thellier-Thellier studies of contacts baked by intrusions or lava flows (*27–29*) have also been used to constrain paleointensities. Although some of these are derived from many samples and therefore might average secular variation, detailed re-

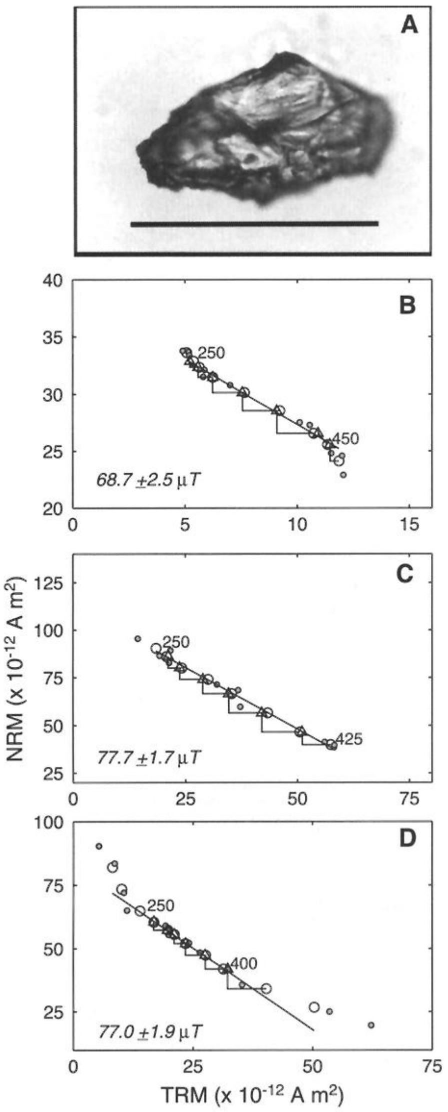

Fig. 2. (**A**) Photomicrograph of typical crystal, scale bar is 1 mm. (**B** to **D**) Typical plots of natural remanent magnetization (NRM) versus thermal remanent magnetization (TRM). pTRM checks are shown by triangles. Large open circles are three-point sliding-window average of raw data (small circles). Labeled points are temperature range (°C) used in least squares fit.

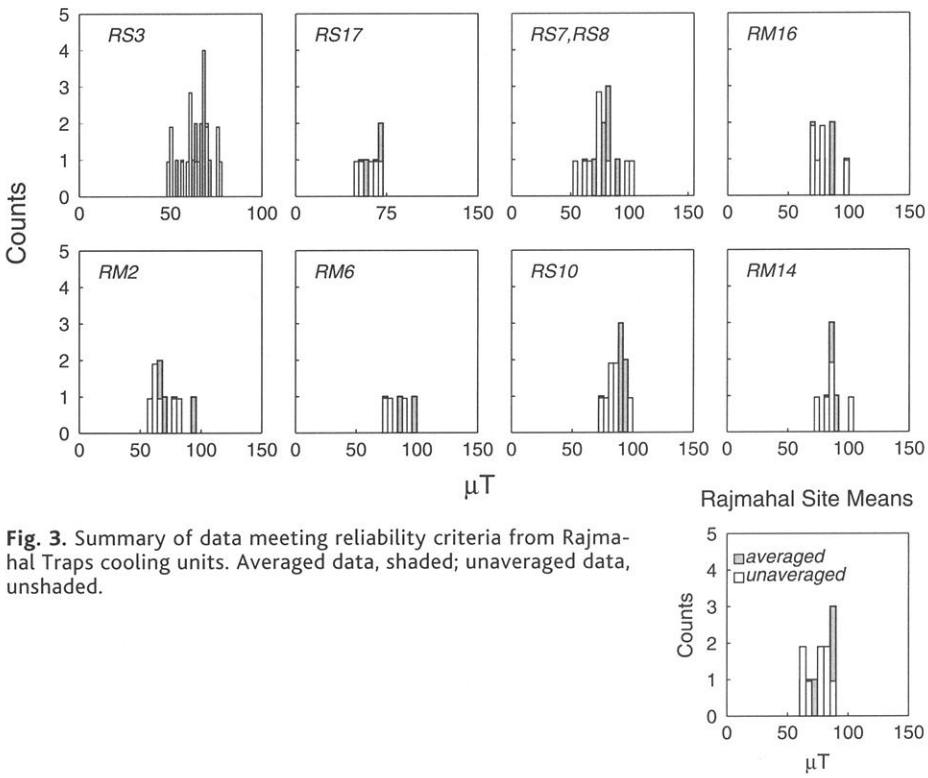

Fig. 3. Summary of data meeting reliability criteria from Rajmahal Traps cooling units. Averaged data, shaded; unaveraged data, unshaded.

sults of reliability tests and coincident paleointensity and directional data have not been published.

Paleointensity results of high technical quality that meet reliability criteria are available from Thellier analyses of submarine basaltic glass (SBG) (*4*, *5*, *30*, *31*). Jurassic to recent results have been reported from samples recovered at Deep Sea Drilling Project (DSDP) and Ocean Drilling Program sites, as well as from the Troodos ophiolite (*5*). The latter yields relatively high paleointensities (*5*) within the Cretaceous Normal Polarity Superchron (~92 Ma, VDM of 7.9 × 10^{22} Am^2, five samples), whereas the former data (*31*) include paleointensities that are low (~111 Ma, DSDP Site 462, VDM of 2.6 × 10^{22} Am^2, three samples). However, these values represent averages of data from individual samples, rather than the averages of independent time units constrained by lava flow stratigraphy and paleomagnetic directional analysis.

Of the SBG data available for the past 180 million years, only eight sites have paleointensity averages based on nine or more samples (*31*). Assuming these determinations are evenly distributed throughout long lava sequences, they should average some secular variation. Two of these results are from sites whose age may be within 1 million years of the marine magnetic anomalies defining the Cretaceous Normal Polarity Superchron (Fig. 4). However, no time-averaged result is available from an interval well within the Superchron corresponding to that represented by our new data. Nevertheless, data available from a few sites based on smaller numbers (one to five samples) of SBG paleointensity determinations (*31*) hint that the standard deviation of the time-averaged field intensity may have changed during the Superchron.

Although the overall database of time-averaged paleointensity values available from basalts, baked contacts, SBG, and plagioclase crystals is relatively small (Fig. 4), a few generalized conclusions can be made. The value we have derived from the Rajmahal Traps is significantly higher than other values available for the past 180 million years and three times that of the mean paleointensity proposed for the Cretaceous to recent time interval (*5*). The range of values from these 113- to 116- Ma samples is also less than that of the past 10 million years (*32*). These observations support some inferences available from recent computer simulations, where the most stable geodynamo (nonreversing, low secular variation) is the most efficient, having the highest dipole moment (*2*). These high intensities may result from latitudinal variations in heat flow across the core-mantle boundary (*2*) or changes in the total heat flow (*33*). Overall, these data from the Cretaceous Normal Polarity Superchron suggest that average paleointensities may be highest when reversal rate is lowest, supporting the idea that reversal rate and paleointensity, rather than decoupled (*3*, *4*, *31*), are governed by the same geodynamic processes (*1*).

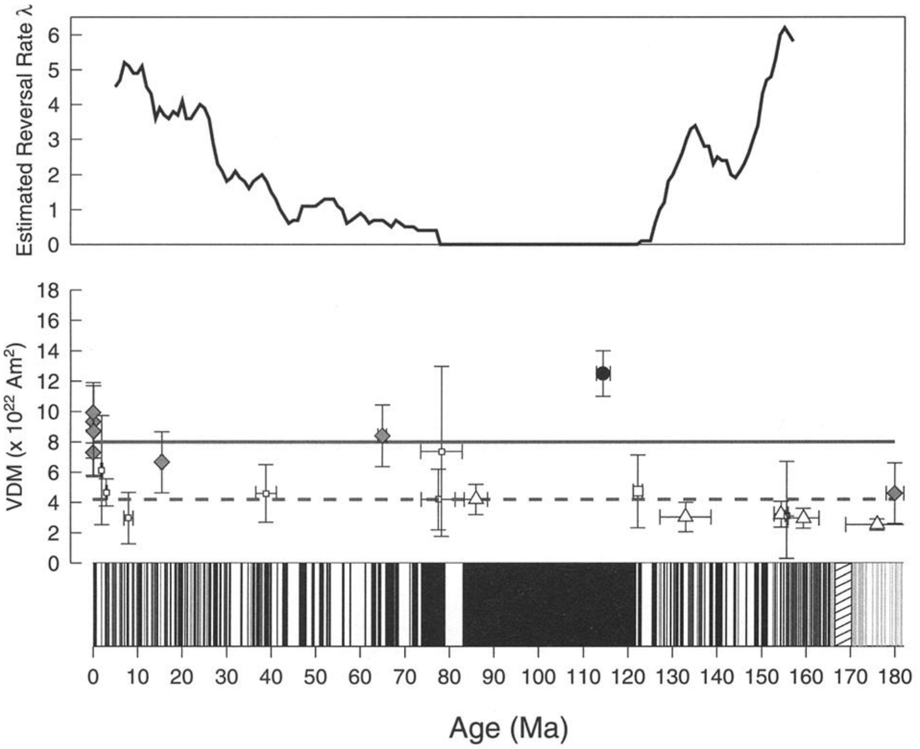

Fig. 4. Geomagnetic reversal time scale (base), select Thellier-Thellier paleointensity results, and estimated reversal rate (based on a 10-million-year sliding window). Geomagnetic time scale to 165 Ma is constrained by marine magnetic anomalies (*34–36*); older reversals (gray) are based on land magnetostratigraphic sections (*36*). Hatched, unambiguous pattern unavailable. Thellier-Thellier determinations, select studies with 1σ errors. Filled symbols are paleomagnetic dipole moments; open symbols are virtual dipole moments. Only studies based on >nine Thellier-Thellier determinations are shown; small symbols, less than 25 samples; large symbols, greater than 25 samples. Data sources: triangles, baked contacts (*27–29*); squares, basaltic glass (*4, 5, 30, 31*); diamonds, basalt whole rocks (*21–26*); circle, basalt plagioclase (this work). Dashed horizontal line: proposed mean Cretaceous-Cenozoic value (*5*). Solid horizontal line: modern field intensity.

References and Notes

1. A. Cox, *J. Geophys. Res.* **73**, 3247 (1968).
2. G. A. Glatzmaier, R. S. Coe, L. Hongre, P. H. Roberts, *Nature* **401**, 885 (1999).
3. M. Prevot, M. E. Derder, M. O. McWilliams, J. Thompson, *Earth Planet. Sci. Lett.* **97**, 129 (1990).
4. T. Pick, L. Tauxe, *Nature* **366**, 238 (1993).
5. M. T. Juarez, L. Tauxe, J. S. Gee, T. Pick, *Nature* **394**, 878 (1998).
6. E. Thellier, O. Thellier, *Ann. Geophys.* **15**, 285 (1959).
7. R. D. Cottrell, J. A. Tarduno, *Earth Planet. Sci. Lett.* **169**, 1 (1999).
8. ———, *J. Geophys. Res.* **105**, 23579 (2000).
9. R. S. Coe, C. S. Gromme, *J. Geomagn. Geoelectr.* **25**, 415 (1973).
10. R. W. Kent, A. D. Saunders, P. D. Kempton, N. C. Ghose, in *Large Igneous Provinces: Continental, Oceanic and Planetary Flood Volcanism*, vol. 100 of *Geophysical Monograph Series*, J. J. Mahohey, M. Coffin, Eds. (American Geophysical Union, Washington, DC, 1997), pp. 145–182.
11. G. J. Sherwood, J. Shaw, *Studia Geophys. Geod.* **35**, 325 (1991).
12. Supplementary data are available at www.sciencemag.org/cgi/content/full/291/5509/1779/DC1.
13. G. J. Sherwood, S. B. Mallik, *J. Southeast Asian Earth Sci.* **13**, 123 (1996).
14. N. I. Fisher, T. Lewis, B. J. J. Embleton, *Statistical Analysis of Spherical Data* (Cambridge Univ. Press, Cambridge, 1987).
15. C. T. Klootwijk, *Tectonophysics* **12**, 449 (1971).
16. P. L. McFadden, R. T. Merrill, M. W. McElhinny, S. Lee, *J. Geophys. Res.* **96**, 3923 (1991).
17. R. S. Coe, *J. Geomagn. Geoelectr.* **19**, 157 (1967).
18. ———, S. Gromme, E. A. Mankinen, *J. Geophys. Res.* **83**, 1740 (1978).
19. The gap factor *g* is defined as $1 - \Delta y/\Delta y_T$, where Δy_T is the length of a NRM-TRM line segment and

$$\Delta y = \frac{1}{\Delta y_T} \Sigma_{i=1}^{N-1} \Delta y_i^2$$

is the weighted mean of the gaps (Δy_i) between points comprising the segment.
20. To test the hypothesis that the means of the averaged and unaveraged paleointensity data for the individual sites are the same, we use a *t* statistic

$$t = \left[(\bar{x} - \bar{y})/s \sqrt{\frac{1}{n_x} + \frac{1}{n_y}} \right]$$

where $\bar{x}$ is the mean of the averaged data, $\bar{y}$ is the mean of the unaveraged data, n_x and n_y are the number of samples for each site (averaged and unaveraged, respectively), and

$$s = \left[\frac{(n_x - 1)s_x^s + (n_y - 1)s_y^2}{n_x + n_y - 2} \right]^{\frac{1}{2}}$$

is a pooled variance (s_x is the error in the averaged data and s_y is the error in the unaveraged data) with ($n_x + n_y - 2$) degrees of freedom.
21. A. Rais, C. Laj, J. Surmont, P.-J. Gillot, H. Guillou, *Earth Planet. Sci. Lett.* **140**, 173 (1996).
22. A. Chauvin, P. Y. Gillot, N. Bonhommet, *J. Geophys. Res.* **96**, 1981 (1991).

23. C. Laj, C. Kissel, *J. Geophys. Res.* **104**, 15317 (1999).
24. M. Prevot, E. A. Mankinen, R. S. Coe, C. S. Gromme, *J. Geophys. Res.* **90**, 10417 (1985).
25. M. Kono, *J. Geophys. Res.* **79**, 1135 (1974).
26. A. Kosterov, M. Prevot, M. Perrin, V. A. Shashkanov, *J. Geophys. Res.* **102**, 24859 (1997).
27. A. S. Bol'shakov, G. M. Solodovnikov, *Izv. Earth Phys. Acad. Sci. USSR (Engl. transl.)* **17**, 754 (1981).
28. ———, *Izv. Earth Phys. Acad. Sci. USSR (Engl. transl.)* **19**, 976 (1983).
29. ———, *Izv. Earth Phys. Acad. Sci. USSR (Engl. transl.)* **23**, 324 (1987).
30. V. Mejia, N. D. Opdyke, M. R. Perfit, *Geophys. Res. Lett.* **23**, 475 (1996).
31. P. A. Selkin, L. Tauxe, *Philos. Trans. R. Soc. London Ser. A* **358**, 1065 (2000).
32. M. Kono, H. Tanaka, in *The Earth's Central Part: Its Structure and Dynamics*, T. Yukutake, Ed. (Terra Scientific, Tokyo, 1995), pp. 75–94.
33. R. L. Larson, P. Olson, *Earth Planet. Sci. Lett.* **107**, 437 (1991).
34. S. C. Cande, D. V. Kent, *J. Geophys. Res.* **100**, 6093 (1995).
35. F. M. Gradstein *et al.*, *J. Geophys. Res.* **99**, 24051 (1994).
36. J. G. Ogg, in *A Handbook of Physical Constants: Global Earth Physics*, T. J. Ahrens, Ed. (American Geophysical Union, Washington, DC, 1995), vol. 1, pp. 240–269.
37. We thank P. K. Bandyopadhyay, S. S. Sarkar, and M. Mukul for assistance in the field. This work was supported by the NSF.

16 November 2000; accepted 16 January 2001

An Antimicrobial Peptide Gene Found in the Male Reproductive System of Rats

Peng Li,[1*] Hsiao Chang Chan,[2*] Bin He,[1*†] Siu Cheung So,[2] Yiu Wa Chung,[2] Quan Shang,[1] You-Duan Zhang,[1] Yong-Lian Zhang[1‡]

Little is known about the innate defense mechanisms of the male reproductive tract. We cloned a 385–base pair complementary DNA and its genomic DNA named Bin1b that is exclusively expressed in the caput region of the rat epididymis and that is responsible for sperm maturation, storage, and protection. Bin1b exhibits structural characteristics and antimicrobial activity similar to that of cationic antimicrobial peptides, β-defensins. Bin1b is maximally expressed when the rats are sexually mature and can be up-regulated by inflammation. Bin1b appears to be a natural epididymis-specific antimicrobial peptide that plays a role in reproductive tract host defense and male fertility.

Reproductive tract infections remain a global public health problem. However, the mechanisms that protect genitourinary organs from ascending infection by sexually transmitted microorganisms, especially along the male reproductive tract, are poorly understood. The epididymis is a male accessory sex organ that consists of a caput (head), corpus (body), and cauda (tail) and is responsible for sperm maturation, storage, and protection (*1*). It may also act as a reservoir of sexually transmitted bacteria and viruses, including human immunodeficiency virus (HIV), as suggested by the fact that epididymitis occurs in 5 to 10% of the sexually active population and can result in 20 to 40% of infected males becoming infertile (*2*). The defensins are innate immune effectors comprising a family of cationic antimicrobial peptides divided into two subfamilies, α-defensins and β-defensins, differing in amino acid sequence, pairing of the six cysteines, and number of exons (*3*). Although defensins are expressed in a wide variety of tissues of different species of vertebrate and invertebrate animals and have been implicated in phagocytic and epithelial host defense (*3*–*6*), none has been found in the epididymis and their role in the male reproductive tract has not been elucidated.

Using differential display analysis of mRNAs (*7*), we cloned a cDNA fragment named Bin1b from the rat epididymis. With two 5′ rapid amplification of cDNA ends (5′-RACE) approaches (*8*), the cap site of Bin1b was identified and its full-length cDNA was 385 base pairs (bp) (excluding the polyadenylate tail), with an open reading frame of 204-bp nucleotides, encoding a 68–amino acid protein (including a 16–amino acid signal peptide) (*9*). This amino acid sequence has 20.3% (14/68) identity with several β-defensins such as bovine neutrophil beta-defensin-9, -3, and -7 found in the cattle (*9*). β-defensins generally have a 60– to 90–amino acid (including a signal peptide) protein precursor, which is digested by endogenous protease into mature functional peptides of 38 to 42 amino acids. Although sequence similarity between Bin1b and the β-defensins appears unimpressive, both the size and structure of Bin1b coincide with the consensus structural characteristics of the β-defensin family (*10*) such that the six cysteine residues are invariantly spaced to form three disulphide bonds and the mature peptide has a net positive charge of +7 (*9*). Furthermore, its cloned and sequenced genomic DNA also exhibited two exons separated by a 1.3-kb intron (*9*). This type of organization is similar to that of other β-defensins reported (*10*).

Unlike other members of β-defensin family, which have been shown to be expressed in a wide array of epithelial tissues, Bin-1b is unique in being epididymis-specific. Of 18 organ tissues examined by Northern blot analysis, Bin1b mRNA was only found in the epididymis (Fig. 1A) and was confined to epithelial cells in the middle part of the caput region (Fig. 1B), as shown by in situ hybridization (Fig. 1, C to E). Monitoring Bin1b expression throughout the life-span of rats indicated that it was developmentally regulated (Fig. 1F). Its expression started at 30 days of age, reached a maximum during the sexually mature period, and then decreased in old rats. Such a region- and development-specific expression pattern of Bin1b suggests its importance in epididymis function and fertility.

The antimicrobial activity of Bin1b was tested with primary cultures of polarized caput and cauda epididymal epithelia by a previously established technique used for studying ion transport properties (*11*). A total of 100 colony-forming units (CFU) of *Escherichia coli* was added to the apical compartment of the epithelial cells after 3 days in culture (0.25×10^6 cells per well), and the medium was collected 16 hours later for CFU counting. No bacterial colony growth was detected in the medium collected from caput cultures, indicating the ability of Bin1b to suppress bacterial colonization, whereas substantial numbers of CFU were observed in the cauda cultures (Fig. 2A). This was consistent with our finding that Bin1b was exclusively expressed in the caput but not the cauda of the epididymis. To confirm that the antimicrobial activity was indeed contributed by Bin1b, we designed antisense oligos of Bin1b and added them to cultures 24 hours before the addition of bacteria. The antibacterial capability

[1]State Key Laboratory of Molecular Biology, Institute of Biochemistry and Cell Biology, Shanghai Institute for Biological Sciences, Chinese Academy of Sciences, 320, Yue-Yang Road, Shanghai 200031, China. [2]Epithelial Cell Biology Research Center, Department of Physiology, Faculty of Medicine, The Chinese University of Hong Kong, Shatin, NT, Hong Kong.

*These authors contributed equally to this work.
†Present address: Laboratories for Reproductive Biology, School of Medicine, University of North Carolina, Medical Sciences Research Building, Campus Box 7500, Chapel Hill, NC 27599, USA.
‡To whom correspondence should be addressed. E-mail: yonglz@sunm.shcnc.ac.cn